15 (2022) 100116

Contents lists available at ScienceDirect

Journal of Non-Crystalline Solids: X

journal homepage: www.sciencedirect.com/journal/journal-of-non-crystalline-solids-x

Alkali and alkaline earth zinc and lead borate glasses: Sintering and crystallization

Lina Heuser *, Marianne Nofz, Ralf Müller

Bundesanstalt für Materialforschung und -prüfung (BAM), Unter den Eichen 87, 12205 Berlin, Germany

ARTICLE INFO

Keywords:
Alkali zinc borate glasses
Lead borate glasses
Viscosity
Sintering
Crystallization
Fragility

ABSTRACT

Glasses in the systems Me_2O-ZnO-B_2O_3 with Me = Li, Na, K, Rb (MeZB), Na_2O-ZnO-CuO-B_2O_3 (NZCuB), CaO-ZnO-B_2O_3 (CaZB), and Li_2O-PbO-B_2O_3 (LPbB) as a reference, were studied by differential thermal analysis, dilatometry, rotational viscometry, and heating microscopy. A decrease of viscosity and sintering range was found with decreasing number of fourfold coordinated boron. The viscosity of the alkali zinc borate glasses varies only slightly. LPbB and CaZB stand out by their reduced and increased viscosities, respectively. Sodium, potassium, and calcium zinc borate glasses possess a fragility above 76. All glasses were sintered to full density before crystallization. Mostly binary zinc borate phases govern crystallization. A ternary crystalline phase was detected only in the potassium containing sample. The Weinberg glass stability parameter ranges between 0.07 and 0.12. This is caused by the presence of several crystalline phases and varying melting points of even the same crystalline phase in different glass matrices.

1. Introduction

Non-toxic ZnO [1,2] is, due to its high polarizability, a promising intermediate oxide to substitute PbO in low-melting borate glasses [3]. These can be used e.g., as sintering aids in Ag-metallization pastes for photovoltaics [4–6] and low temperature cofired ceramics (LTCC) [7,8], or in soldering and sealant applications [1,9]. Different alkali zinc borate glasses were studied as models for leadfree silver metallization paste glasses by Körner [6].

A thorough understanding of the relations between composition, structure, and properties is necessary for the development of novel alkali or alkaline earth zinc borate glasses for low-temperature applications. The effect of alkali and alkaline earth ions on viscosity, sintering, and crystallization is of special interest. However, such data are very rare. Danewalia et al. [9] and Saidu et al. [10] published results of thermal analyses of Li_2O-ZnO-B_2O_3 glasses. Gaafra et al. [11] reported glass transition temperatures of the (1-x)[29Na_2O-4Al_2O_3-67B_2O_3]-xZnO glass system. The structure of Me_2O-ZnO-B_2O_3, Me = Li, Na, K, Rb (MeZB), Na_2O-ZnO-CuO-B_2O_3 (NZCuB), CaO-ZnO-B_2O_3 (CaZB) and Li_2O-PbO-B_2O_3 (LPbB) glasses was determined by means of Raman and IR spectroscopies as given in a previous work [12]. As a result, the glasses were distinguished with respect to the formation of either pentaborate groups in the networks of i.) LZB, NZB, NZCuB, and CaZB or diborate groups in the networks of ii.) KZB, RZB, and RZB1 [12]. For LPbB both borate groups were indicated [12]. LPbB served as reference to study the effect of substitution of lead oxide by zinc oxide.

The present work aims to i.) evaluate viscosity, sintering and crystallization of the glasses with respect to the potential application as sintering aid and ii.) to discover the role and influence of network modifiers and intermediate oxides on these properties. For that purpose, glasses studied in [12] were investigated with differential thermal analysis, dilatometry, rotational viscometry, and heating microscopy.

2. Experimental

2.1. Samples

Zinc borate glasses Me_2O-ZnO-B_2O_3, Me = Li, Na, K, Rb (MeZB), Na_2O-ZnO-CuO-B_2O_3 (NZCuB), and CaO-ZnO-B_2O_3 (CaZB) with compositions taken from [12] are listed in Table 1. Additionally, a Li_2O-PbO-B_2O_3 (LPbB) glass serves as a reference.

2.1.1. Glass melts

For glass preparation the raw materials B_2O_3 (99%, Alfa Aesar/ThermoFisher (Kandel) GmbH, Kandel, Germany), Li_2CO_3 (Emplura ≥98.5%, Merck KGaA, Darmstadt, Germany), Na_2CO_3 (Ensure ISO ≥

* Corresponding author.
E-mail address: Lina.Heuser@bam.de (L. Heuser).

https://doi.org/10.1016/j.nocx.2022.100116
Received 1 July 2022; Received in revised form 24 August 2022; Accepted 25 August 2022
Available online 29 August 2022

99.9, Merck KGaA, Darmstadt, Germany), K_2CO_3 (p.a. ≥ 99.9%, Merck KGaA, Darmstadt, Germany), Rb_2CO_3 (99%, ChemPUR GmbH, Karlsruhe, Germany), $CaCO_3$ (p.a. ≥ 99.5%, Merck KGaA, Darmstadt, Germany), ZnO (≥ 99%, Carl Roth GmbH, Karlsruhe, Germany), PbO (p.a. ≥ 99%, yellow, Honeywell, Fluka, Seelze, Germany) and CuO (p.a. ≥ 99%, Honeywell, Fluka, Seelze, Germany) were used.

For LZB, NZB, KZB, and RZB1, batches of 1.70–3.50 kg were melted in Pt/Rh 20 crucibles in an inductively heated furnace (Ema Tec 2002, EMA Tec GmbH, Sondershausen, Germany) at 1100 °C for 1 h. Batches of 0.05 kg to 0.45 kg were melted at 1250 °C for 1 h in Pt/Rh 20 crucibles for CaZB, at 950 °C for 1 h in Al_2O_3 crucibles for LPbB, at 1100 °C for 1 h in Al_2O_3 crucibles for NZCuB, and at 1100 °C for 1 h in Pt/Rh 20 for RZB using a high temperature laboratory furnace VMK1800 (Linn High Therm GmbH, Eschenfelden, Germany). Except CaZB, all glass melts were quenched in water to avoid crystallization and the frits were remelted to achieve homogenization, see paragraph 2.1.2. Glass frits were used for powder preparation.

2.1.2. Bulk glass samples

To obtain bulk glass samples, glass frits were remelted and casted onto steel molds. Due to its strong crystallization tendency, the LZB melt was casted onto a copper mold. The CaZB melt was directly casted onto a steel mold. All bulk glasses were cooled from T_g + 20 K to room temperature in a switched off electrical chamber furnace.

2.1.3. Glass powders and compacts

Dry milling of glass frits in air was performed for 12 min utilizing a planetary micro mill (Pulverisette 7, Fritsch, Idar-Oberstein, Germany). Zirconium oxide (ZrO_2) grinding jars were loaded with glass frits and 10 mm ZrO_2 balls. The dry milled glass powders were then exposed to wet milling in isopropanol under the same conditions but using 3 mm ZrO_2 milling balls. Particle size data are shown in Table 2. After wet milling, the glass powders were sieved to <300 µm for thermal analysis and sintering studies to diminish particle agglomeration. A fine particle size was necessary due to the technological background i.e., preparation of silver pastes.

Cylindrical compacts (diameter ≈ height ≈ 5 mm) were uniaxially pressed with 25 MPa for 30 s and used for XRD and sintering studies with heating microscopy (HM). The compact densities (ρ_0) calculated from sample dimension and weight data within 3% accuracy are shown in Table 2. For XRD measurements, compacts were heated at 5 K/min to 700 °C and quenched in air. The annealed glass powders were sieved to <63 µm. Prior to HM, the compacts were heated to 300 °C (LPbB) or 400 °C (all other samples), held for 30 min and cooled to room temperature in the furnace. Thus, water release did not contribute to the shrinkage curves shown below.

2.2. Methods

2.2.1. Particle size

Particle size measurements were performed using Mastersizers 2000 and 3000 (Malvern-Panalytical GmbH, Kassel, Germany). The glass powders were dispersed in isopropanol and disagglomerated by ultrasonic treatments for 5 min.

Table 2
Particle size distributions of wet milled glass powders in µm and initial relative compact density values used for sintering studies.

Glass	d_{10}	d_{50}	d_{90}	ρ_0
LZB	0.69	2.08	6.41	0.51
NZB	1.62	3.51	9.09	0.55
KZB	1.51	3.35	7.07	0.52
RZB	2.19	4.84	11.1	0.54
RZB1	2.01	4.37	11.2	0.55
LPbB	0.95	2.56	6.23	0.53
CaZB	1.16	2.82	6.12	0.51
NZCuB	1.35	3.15	6.61	0.50

2.2.2. Gas release (VHE)

The degassing of the RZB glass powder (< 300 µm) was analyzed using a vacuum hot extraction device (VHE) coupled with a mass spectrometer (QMA4005, Balzers Instruments, Balzers, Liechtenstein). VHE analysis was accomplished in vacuum (10^{-5}–10^{-7} mbar) during heating at 10 K/min utilizing the multiple-ion detection mode.

2.2.3. Differential thermal analysis (DTA)

Crystallization of glass powders (<300 µm) was studied with differential thermal analysis (DTA) combined with thermogravimetry (TG) (TGA 24, Setaram, Caluire, France). Glass powders (10 mg–25 mg) were heated at 5 K/min to 1000 °C in air. This heating rate was selected to be similar to the one used for the sintering studies. In case of LPbB, corundum crucibles and for all other samples platinum crucibles were used.

2.2.4. X-ray diffraction (XRD)

Crystalline phases were analyzed with an X-ray diffractometer (D8 ADVANCE, Bruker AXS, Karlsruhe, Germany) utilizing CuKα_1 & Kα_2 radiation. The diffractometer featured a LYNXEYE XE-T detector in Bragg-Brentano-Geometry. Data were recorded for $2\theta = 3° - 80°$ in steps of 0.02°. Diffraction patterns were analyzed using the software EVA V 5.0 (Bruker-AXS, Karlsruhe, Germany) and compared to ICSD database (ICSD, 2019, FIZ, Karlsruhe, Germany) [13].

2.2.5. Viscosity (η)

Low viscosity (< 10^4 Pa·s) was measured with a rotational viscometer (Viskotester VT550, Haake GmbH, Erlangen, Germany) equipped with a cylindric stirrer for viscometry measurements of NZB, KZB, and CaZB based on standards [14,15]. Glass frits were melted at 1100 °C (1250 °C for CaZB) and then stepwise cooled to different temperatures, where the torque was measured at 0.5, 1, 3, 5, 10, 30, 50, and 80 rpm for 1 min. Measurement uncertainty was < ± 0.06 log η (η in Pa·s) and temperature uncertainty was ±8 °C obtained from calibration with the standard NIST 710a.

Medium viscosity (10^7–10^{10} Pa·s) was measured by means of the cylinder compression method. The measurements were performed according to ASTM C1351M - 96 (Reapproved 2017) [16]. Cylindrical samples of 5 mm in diameter and height were heated at 5 K/min to selected temperatures in a vertical dilatometer (TMA 801, Bähr-Thermoanalyse GmbH, now TA Instruments, Hüllhorst, Germany). After

Table 1
Chemical compositions of the glasses under study in mol% and glass densities (ρ_G) in g/cm^3 [12].

Glass	B_2O_3	ZnO	Li_2O	Na_2O	K_2O	Rb_2O	CaO	PbO	CuO	ρ_G
LZB	53.2	26.9	19.9							2.829
NZB	53.7	26.4		19.9						2.788
KZB	53.3	27.6			19.1					2.632
RZB	53.5	27.1				19.4				3.020
RZB1	58.9	26.2				14.9				2.996
LPbB	55.3		19.5					25.2		3.764
CaZB	49.5	31.1					18.4			3.103
NZCuB	52.6	21.9		20.8					4.7	2.764

reaching the first selected measuring temperature, the sample was exposed to a dwell time of 45 min for glass relaxation. The dwell time prior to the following measurements was 15 min. For isothermal measurements, a load between 0.5 and 1.25 N was applied for 20 min. After each measurement, the sample was heated at the same heating rate to the next temperature. To be sure, that the measurements are not affected by crystallization, the sample was finally cooled at 5 K/min to the first temperature and was measured again. Measurement uncertainty was <0.01 log η (η in Pa·s) and temperature deviation was ±5 °C.

Viscosity data were fitted with the MYEGA equation [17], where T_{12} is defined by log η(T_{12}) = 12 (T_g as used in [18]), L_∞ is the high temperature limit of log η, and m the fragility of the glass forming melt. T_{12} was approximated with the dilatometric glass transition temperature taken from [12]. Calculations were performed using temperatures (T) in Kelvin (K) and Eq. (1).

$$log\ \eta(T) = L_\infty + (12 - L_\infty)\cdot\frac{T_{12}}{T}\ exp\left[\left(\frac{m}{12 - L_\infty} - 1\right)\cdot\left(\frac{T_{12}}{T} - 1\right)\right] \quad (1)$$

2.2.6. Heating microscopy (HM)

Sintering of cylindrical glass-powder-compacts was analyzed by means of a heating microscope (Leitz, Wetzlar, Germany) with optical data acquisition (Hesse Instruments, Osterode, Germany) during heating at 5 K/min. The sample temperature was measured within 8 K accuracy. Shrinkage is presented in terms of the linear isotropic shrinkage, s. To visualize the respective degree of densification, the relative density, ρ, is also presented in Fig. 2 (right ordinate). Shrinkage s was obtained from the compact height, h, and the silhouette area data, A, assuming ideal cylindrical geometry and isotropic sintering. In this case, the compact volume V is $\frac{A^2\cdot\pi}{4\cdot h}$ and the relative density equals ρ = (m/V)/ρ_G, where ρ_G is the glass density. s is related to ρ according to Eq. (2) [19,20]:

$$s = 1 - \sqrt[3]{\frac{\rho_0}{\rho}} = 1 - \sqrt[3]{\frac{(\rho_C/\rho_G)}{\rho}} \quad (2)$$

where, ρ_0 and ρ_C are the initial relative density and the absolute density of the compact, respectively. For example, for ρ_0 = 0.55 a maximum shrinkage of 0.18 can be expected from Eq. (2) with ρ = 1. Since in Eq. (2) s depends on ρ_0, experimental scatter in ρ_0 for different compacts was corrected according to Eq. (3)

$$s_{corr} = \left(\left[1 - \sqrt[3]{\frac{\langle\rho_0\rangle}{1}}\right] \Big/ \left[1 - \sqrt[3]{\frac{\rho_0}{1}}\right]\right)\cdot s \quad (3)$$

with $\langle\rho_0\rangle$ = 0.55. Compact density was calculated from measured data for h, A, and the compact weight. Glass density ρ_G was taken from [12] (Table 1).

3. Results

3.1. Viscosity

Fig. 1 shows measured viscosity data (symbols) for the glasses under study. For LZB, RZB, RZB1, NZCuB, and LPbB, high temperature viscometry was prevented by crystallization or technical reasons. The curves of the other samples were fitted with Eq. (1) and Table 3 lists the best fitting parameters.

Most strikingly, all log η(T) curves have a quite similar slope, i.e., similar fragility m, although the temperature for a given viscosity value varies.

3.2. Sintering

Fig. 2 shows the isotropic linear shrinkage (s) for the borate glass powder compacts (left ordinate) and the corresponding relative compact density (ρ) (right ordinate).

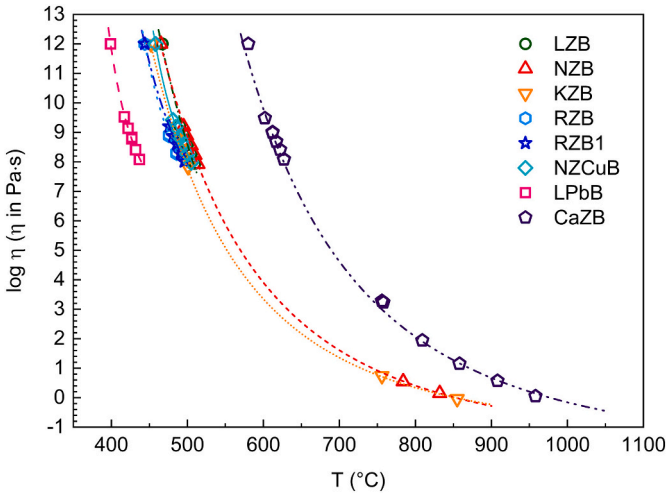

Fig. 1. Viscosity data (symbols) measured by means of dilatometry with cylinder compression (log η = 7–10) and rotational viscometry (log η < 4), T_{12} taken from ref. [12]. For glasses NZB, KZB, and CaZB curves were fitted with Eq. (1). Table 3 lists the fitting parameters. For the other samples lines serve as guide for the eyes.

Table 3
Parameters used in Eq. (1) for viscosity fitting in Fig. 1. T_{12} in °C is taken from ref. [12]. The uncertainty of the fit is denoted as dL and R^2 is the correlation coefficient.

Parameter	NZB	KZB	CaZB
$-L_\infty$	1.895	1.499	2.195
T_{12}	465	452	580
m	77	80	77
dL	0.04	0.07	0.18
R^2	0.9999	0.9997	0.9981

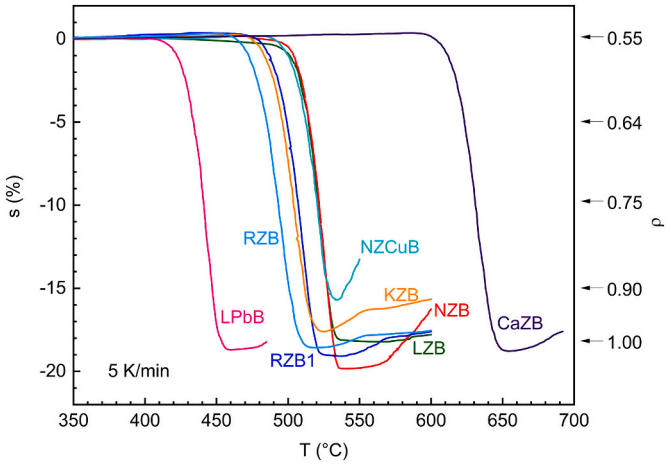

Fig. 2. Isotropic linear shrinkage of powder compacts (s) and corresponding relative density (ρ) according to Eqs. (2) and (3).

Table 4 summarizes characteristic sintering temperatures. All powders reach almost full densification (ρ > 0.9). As the only exception, the NZCuB compact foamed up right after shrinkage. As expected from viscosity behavior displayed in Fig. 1, all samples show a similar slope, although sintering temperatures largely scatter. Consistent with Fig. 1, the lowest value for $T_{s\text{-}on}$ belongs to LPbB (417 °C), medium values are found for the alkali zinc borate glasses (469–500 °C) and the maximum

Table 4
Sintering onset temperatures ($T_{s\text{-}on}$), taken at s = − 0.5%, and densification temperatures ($T_{s\text{-}end}$), taken at the minimum of s(T). All temperatures are given in °C.

Glass	$T_{s\text{-}on}$	$T_{s\text{-}end}$
LZB	492	535
NZB	500	535
KZB	480	523
RZB	469	513
RZB1	483	523
LPbB	417	460
CaZB	608	650
NZCuB	496	535

Table 5
Fictive temperatures (T_f), crystallization onsets (T_C), melting onset temperatures (T_m), and melting endpoints (T_l), data taken from Fig. 3. All temperatures are given in °C.

Glass	T_f	T_C	T_m	T_l
LZB	472	545, 607	734, 815	841
NZB	456	564	752	855
KZB	453	555, 600	798	807
RZB	446	550	678, 808, 845	929
RZB1	443	559	718, 787, 837	877
LPbB	390	504	631	792
CaZB	574	700, 780	828, 856	1010
NZCuB	454	579	728	753

value is observed for CaZB (608 °C). Relative densities above 1.00 are due to the systematic error of the heating microscopy, which is neglectable in the present study.

3.3. Crystallization

Fig. 3 shows the results of thermal analysis of the glasses under study. Fictive temperatures (T_f), crystallization onsets (T_C), melting onset temperatures (T_m), and melting endpoints, i.e., liquidus temperatures, (T_l) are marked with arrows and are listed in Table 5. The weak shoulders between T_f and T_C most likely reveal sintering as indicated by T_s (compare Table 4). Comparison with DTA curves of compact samples (not shown) verifies the assignment of T_s to sintering. Consistent with Fig. 2, which indicates full densification for all glass powders, primary crystallization starts after densification and T_C - $T_{s\text{-}end}$ ranges between 10 K (LZB) and 50 K (CaZB). Nevertheless, all glasses under study obviously undergo crystallization and show at least one crystallization and one melting peak.

Fig. 4 and Table 6 show the XRD results for glass samples which were heated to 700 °C. This temperature was chosen since crystallization surely appeared in all samples. XRD main peaks taken from the powder diffraction files [21–27] are designated by different symbols in Fig. 4. For the sake of clarity small peaks from pdf data were left out, e.g., for $KZnB_3O_6$ out of the 85 peaks only 17 intense peaks are marked.

The zinc borate phase $3ZnO{\cdot}B_2O_3$ dominantly occurs in the crystallized sample of LZB and is clearly detectable for NZB as well as for NZCuB. Whereas for LZB and NZB the low temperature polymorph α-$3ZnO{\cdot}B_2O_3$ (☆) was identified, the high temperature ß-$3ZnO{\cdot}B_2O_3$ polymorph was found for NZCuB (○). For LZB, the presence of $ZnO{\cdot}B_2O_3$ (+), $ZnO{\cdot}2B_2O_3$ (◊), and $Li_2O{\cdot}2B_2O_3$ (□) is also shown. In LPbB, only $Li_2O{\cdot}2B_2O_3$ was found. Additionally, metallic lead or lead containing phases are possible for LPbB (not labelled). In KZB, the only ternary phase, $KZnB_3O_6$ (△) was found. The crystal structure and metaborate groups containing crystalline network were shown by Jin et al. [28]. Further borate phases were checked for the glasses under study but could not be surely assigned to the diffraction patterns. Since not all XRD peaks could be assigned, it can be assumed, that phases, which have still not been characterized or are not contained in the ICSD database [13] crystallized in the glasses under study.

3.4. Degassing

Fig. 5 exemplarily shows the degassing of the RZB glass powder during heating at 10 K/min. Below T_g, degassing is clearly dominated by water, in particular below 200 °C. The TG measurement (dashed-dotted curve) shows that the main mass loss occurs in this temperature region. Around T_g, H_2, O_2, N, CO_2, C and CO or/and N_2 degassing is detected as well. The sharp drop of degassing activity between 480 and 500 °C well coincides with the sintering range shown in Fig. 2. Above 600 °C, degassing spikes indicate the degassing of carbon gases as it was reported for other glasses as well [29–31].

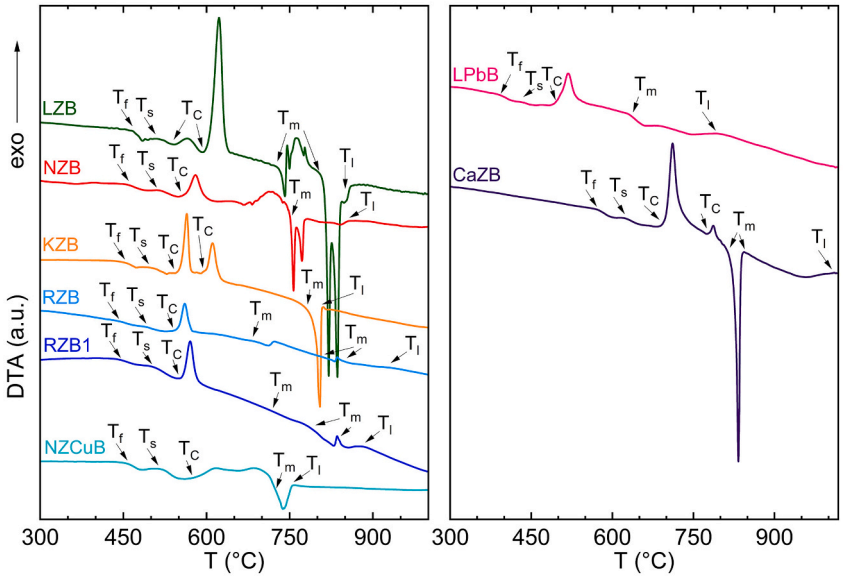

Fig. 3. DTA curves with indication of fictive temperatures (T_f), sintering temperatures (T_s), crystallization temperatures (T_C), melting onset temperatures (T_m), and melting endpoints (T_l).

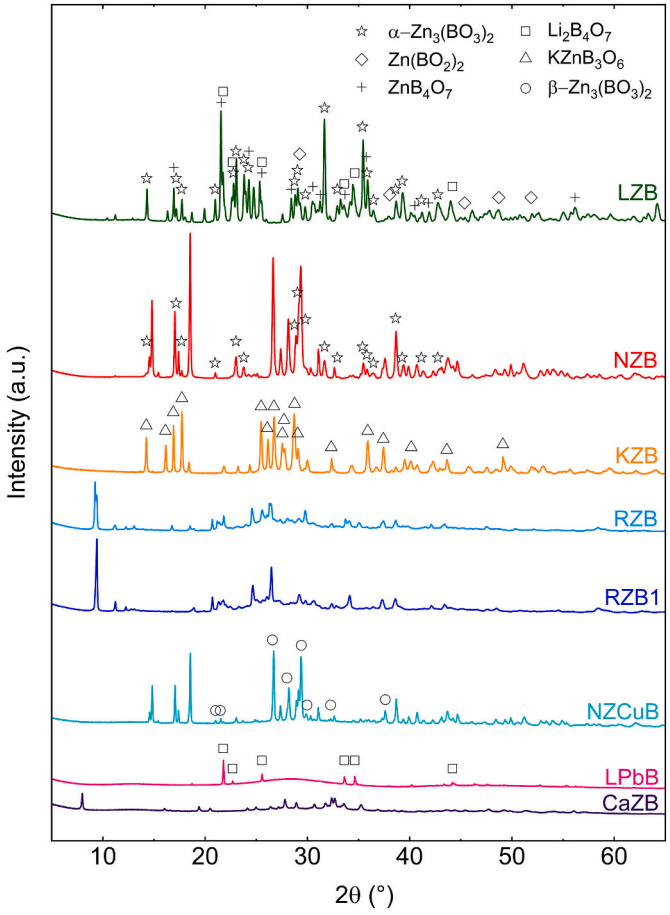

Fig. 4. XRD patterns of crystallized borate glasses heated to 700 °C at 5 K/min. See Table 6 for crystal structure details.

4. Discussion

4.1. Viscosity and sintering

Fig. 1 shows the viscosities of the glasses under study, where LPbB and CaZB stand out for their small and large viscosity, respectively. The exceptionally low viscosity of LPbB is reasonable due to the high polarizability of Pb^{2+} [1,32]. As outlined by Bobkova and Khot'ko [1] a relation between degree of screening of the positive nucleus by electrons or cations and the melting temperature exists. Furthermore, the degree of screening depends on the polarizability of the ions [1]. Hence, higher polarizability results in a lower viscosity [1]. Also Zn^{2+} ions are highly polarizable, but their higher field strength is responsible for the comparably higher viscosity, as described by Scholze [32].

CaZB has the highest viscosity. Although the number of fourfold coordinated boron atoms, N_4, is similar for CaZB and LZB glasses [12], the viscosity-temperature curve is shifted to >100 K higher temperature. Chryssikos et al. and Yiannopoulos et al. [33,34] ascribed the higher T_g of Ca-borate glasses compared to Li-borate glasses to the higher "crosslinking" potential and coordination number of Ca^{2+}. This explanation also applies to viscosity.

Viscosity slightly decreases with increasing alkali ion radii (Fig. 1). This effect can be attributed to the slight decreasing tendency to support fourfold boron coordination at the expense of nonbridging oxygen (NBO) discussed in [12]. The equilibrium between the formation of either B_4-units or NBOs and B_3-units depends on a combination of alkali ion properties [35,36]. These are the basicity [35,37,38], the ionic radius, related steric effects, and the polarizability [35].

Additionally, the high, constant Zn^{2+}-content [12] and the large contribution of these ions to formation of NBOs can diminish the influence of the type of alkali ions. The slight decrease in viscosity of NZCuB compared to NZB could be due to the role of Cu^{2+} as network modifier whereas Zn^{2+} partially acts as network former [39].

Fig. 6 displays the Angell plot of the viscosity data for which high temperature measurements were not prevented by crystallization shown in Fig. 1. Curves are calculated with Eq. (1). Viscosity data for B_2O_3 are taken from [40,41]. The fitting parameters for B_2O_3 are $-L_\infty = 0.106$, $T_{12} = 277$ °C, m = 47.3, dL = ± 0.08 and $R^2 = 0.9994$.

The fragility parameters [17,42,43], reflecting the temperature effect at T_{12} according to Eq. (4),

$$m = \left.\frac{\partial log\eta(T)}{\partial(T_{12}/T)}\right|_{T=T_{12}} \quad (4)$$

vary slightly between 77 and 80 for NZB, KZB, and CaZB (Table 3) indicating "fragile" behavior, i.e., a strong effect of temperature. For comparison, the "strong" glass former B_2O_3 with m = 47 essentially

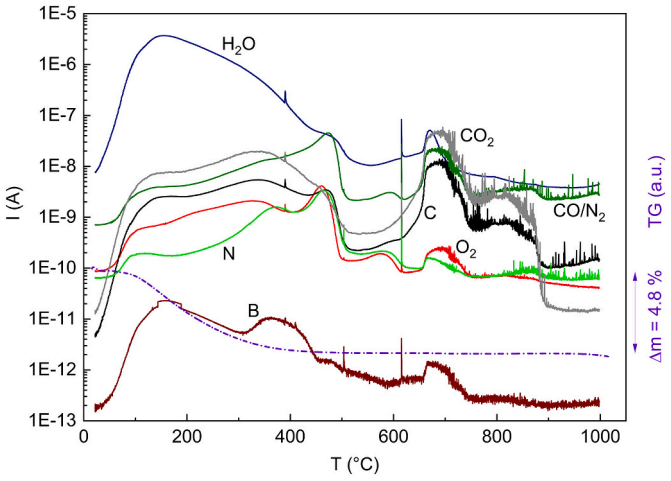

Fig. 5. Degassing in terms of ion current (I) vs. temperature (T) for a RZB glass powder heated at 10 K/min. Sample mass = 54 mg.

Table 6
Crystal phases, occurrence, and structure data.

Crystal phases	Symbols	Glasses	Borate groups	Structures	PDFs
$Zn_3(BO_3)_2$	☆	LZB, NZB	Orthoborate	Triclinic (low temperature α-polymorph)	01–075-3037 [21]
$3ZnO{\cdot}B_2O_3$	○	NZCuB	Orthoborate	Monoclinic (high temperature ß-polymorph) [21]	00–027-0983 [22,23]
ZnB_4O_7	+	LZB	Diborate	Orthorhombic	01–071-0634 [24]
$ZnO{\cdot}2B_2O_3$					
$Zn(BO_2)_2$	◊	LZB	Metaborate	Cubic	00-039-1126 [25]
$ZnO{\cdot}B_2O_3$					
$Li_2B_4O_7$	□	LZB, LPbB	Tetraborate	Tetragonal	01-077-6271 [26]
$Li_2O{\cdot}2B_2O_3$					
$KZnB_3O_6$	△	KZB	Metaborate [28]	Triclinic	00–060-0860 [27]
$K_2O{\cdot}2ZnO{\cdot}3B_2O_3$					

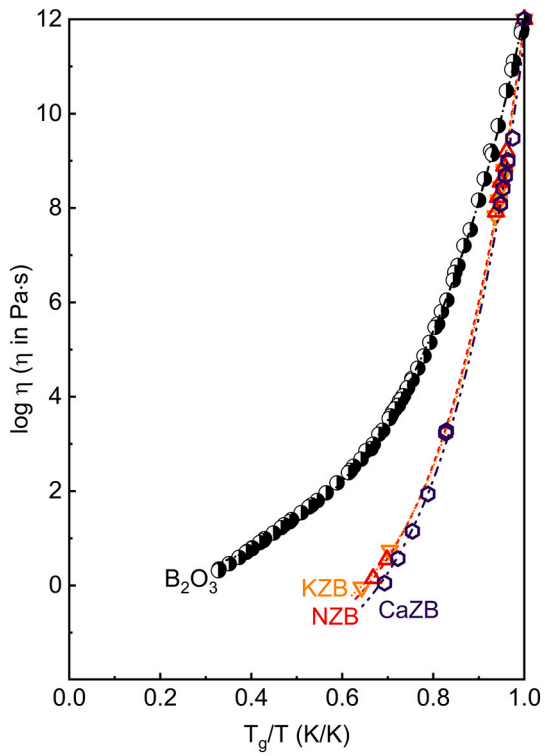

Fig. 6. Angell plot of viscosity versus T_g/T for NZB, KZB, CaZB, and B_2O_3. Curves are calculated with Eq. (1). Viscosity data for B_2O_3 are taken from [40,41]. The symbols indicate the experimental data points.

deviates. B_2O_3 is a strong glass forming liquid due to the high connectivity [44] and low fluctuation of the coordination number [45]. The type of alkali or alkaline earth ions in the zinc borate glasses under study does not significantly affect the fragility, since N_4, thus the level of network connectivity, and the fluctuation of the coordination number of boron vary only slightly. The weak effect of alkali and even alkaline earth ions on fragility is consistent with similar findings on binary alkali and alkaline earth borate glasses, which was discussed to result from a competition between crosslinking induced by B-O and M-O bonds [33]. This competition is induced by opposite trends of coordination number and N_4 [12] in relation to the ionic radius, that also holds for the (alkali and calcium) zinc borate glasses. Mauro et al. [46] calculated fragilities of maximum 80 for the binary lithium and sodium borate glasses with up to 50 mol% modifier. The here found fragilities are in the same range. This is a hint to the role of the zinc ions as network modifiers, i.e., formation of NBO by zinc ions corresponds with formation of NBO by enhanced alkali content. Action of a majority of Zn^{2+} ions as network modifier was also concluded from spectroscopic studies presented by Heuser and Nofz [12].

The glass sintering occurs by viscous flow, which is directly proportional to the surface tension and inversely proportional to the viscosity and particle radius [19]. The surface tension of the glasses under study is unknown. The influence of the alkali ions on the surface tension of binary borate glass melts was found to be low [47]. Hence, it can be assumed, that this also applies to the alkali zinc borate glasses. The particle radii are kept approximately constant (Table 2). The onset of viscous flow and thus sintering are related to a viscosity of $\log \eta \approx 9$ (η in Pa·s) consistent with Scholze [48]. The respective temperature depends on the glass composition. For alkali zinc borate and NZCuB glasses, sintering starts in a narrow temperature range of 31 °C. This is due to the small differences in viscosity. Thus, a minor effect of the different alkali ions and of Cu^{2+} on sintering was found for the glasses under study (see Fig. 2, Table 4). The presence of Ca^{2+} leads to a higher viscosity and a sintering start at higher temperature compared to the alkali zinc borate series. The lower viscosity of LPbB results in earlier sintering than measured for LZB.

All samples are fully densified before crystallization starts (compare $T_{s\text{-end}}$ (Table 4) and T_C (Table 5)). Thus, the glasses under study are suitable as sintering aids. Thermally induced processes after densification can be identified with the help of the DTA curves and shadow images of the samples. Thus, plateaus and increasing curves can be interpreted as crystallization and softening. To give an example, the increase of the KZB curve between 525 °C and 550 °C is caused by softening and the following plateau is governed by crystallization. The strong increase of the curve of NZCuB originates from softening combined with foaming.

An additional remark is necessary regarding the degassing. Körner [6] found an early shrinkage in rubidium containing glasses. That finding could be explained by the water release, indicated by the VHE analysis shown in Fig. 5. The water release leads to ~5% mass loss, which results in earlier shrinkage in the sintering curve. The strong hygroscopic behavior of rubidium oxide increases the water content in these glasses. Heating the glass powders first to 400 °C (below T_g) before sintering studies avoided the effects described above (see Fig. 2).

4.2. Glass stability

Although Fig. 2 indicates full densification for the fine glass powder fractions studied here, the discussion of glass stability in terms of glass transition and crystallization temperatures T_g and T_C, respectively, may provide useful information about processing tolerances in glass melting or sintering. For this purpose, the Weinberg glass stability parameter [49] was calculated according to Eq. (5) from respective absolute temperature data (K) given in Table 5 and Fig. 3.

$$K_W = \frac{T_C - T_g}{T_m} \tag{5}$$

T_f was used instead of T_g in the calculations here to ensure that glass transition and crystallization temperatures refer to the same heating rate. Following Nascimento et al. [50], who found that crystallization onset temperatures provide better results, we used the onset temperature T_C in Eq. (5) instead of the crystallization peak temperature as done in [49]. Due to the crystallization and melting of mostly more than one crystalline phase in each glass melt, only the first crystallization peak was utilized. The melting endpoint T_l instead of T_m was chosen for calculation according to Ferreira et al. [51].

Fig. 7 presents the calculated K_W parameters for the glass powders under study. LZB has the lowest value, whereas K_W is almost similar for the calcium containing one and the other alkali zinc borate glasses. LPbB shows a higher value for K_W than LZB. This clearly indicates the increase of glass stability by substitution of Zn^{2+} by Pb^{2+}. Similarly, the partial

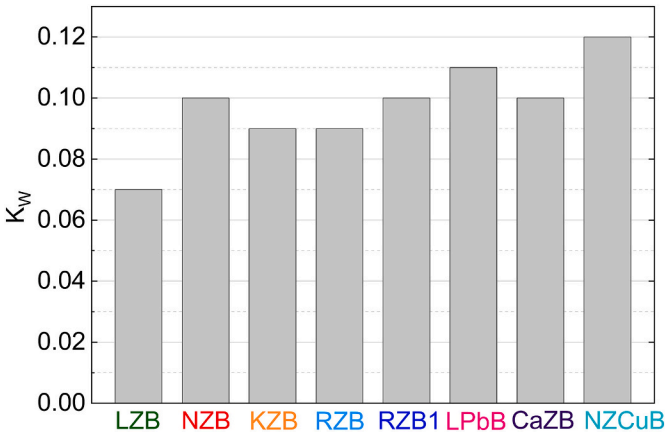

Fig. 7. Glass stability parameter (K_W).

replacement of Zn^{2+} by Cu^{2+} results in an increase of glass stability as also discussed by Yao et al. [39].

4.3. Glass crystallization

The crystal phases identified after heating the glass powders under study to 700 °C (Fig. 4) are summarized in Table 6. It is interesting to note that the binary zinc borates, $3ZnO{\cdot}B_2O_3$ (☆,○), $ZnO{\cdot}B_2O_3$ (◇), and $ZnO{\cdot}2B_2O_3$ (+), favorably crystallize in LZB. For temperatures of 640 °C–700 °C Whitaker [52] confirmed the existence of α-$3ZnO{\cdot}B_2O_3$ and $ZnO{\cdot}2B_2O_3$. α-$3ZnO{\cdot}B_2O_3$ is the main phase and only minor amounts of $ZnO{\cdot}B_2O_3$ are present in LZB. Additionally, the alkali containing phases $Li_2O{\cdot}2B_2O_3$ (□) and $K_2O{\cdot}2ZnO{\cdot}3B_2O_3$ (△) were found in the respective glasses.

$3ZnO{\cdot}B_2O_3$ was identified in three samples although its chemical composition is most far from that of the glasses under study. This phase is dominating in LZB as well as in NZB in its low temperature α-polymorph (☆), and in NZCuB in its high temperature β-polymorph (○). This finding indicates that the partial substitution of ZnO by CuO has hindered the high-low temperature transformation during cooling. Such hindrance is also supported by the weaker and broader crystallization and melting peaks observed in NZCuB. The appearance of more than one crystalline phase in most samples explains the multiple melting peaks in the DTA curves.

Edge-sharing (es) $K_2O{\cdot}2ZnO{\cdot}3B_2O_3$ with es-BO_4 was detected in KZB as the only ternary phase (Fig. 4). An isostructural phase to $K_2O{\cdot}2ZnO{\cdot}3B_2O_3$ could not be synthesized with other alkali ions [28]. The sharp melting peak of $K_2O{\cdot}2ZnO{\cdot}3B_2O_3$ at 802 °C [28] fits the melting peak of KZB at 798 °C (Table 5, Fig. 3). Since Jin et al. [28] did not measure any additional peak, the second exothermic peak in the DTA curve of KZB (Fig. 3) could hint to a second crystalline phase. With regard to the stoichiometry the additional crystallization of $K_2O{\cdot}2B_2O_3$ has to be considered. However, the XRD pattern of KZB at 700 °C indicates the crystallization of only one phase. A solid-solid phase transition from a metastable to a stable phase could also be an explanation for the second exothermic DTA-peak. It is conceivable, that $K_2O{\cdot}2ZnO{\cdot}3B_2O_3$ undertakes a phase transition, when crystallization proceeds in a glassy matrix. Jin et al. [28] and Yang et al. [53] calculated a hypothetical corner-sharing (cs) $K_2O{\cdot}2ZnO{\cdot}3B_2O_3$ to be less geometrically and energetically stable.

Two groups of the alkali zinc borate glasses under study can be distinguished with regard to the formation of pentaborate groups in LZB, NZB, and NZCuB and diborate groups in KZB, RZB, and RZB1 [12]. Correspondingly, LZB and NZB show similar crystallization behaviors: i.) the main phase is $3ZnO{\cdot}B_2O_3$ and ii.) the melting and crystallization peaks are superimposed (see Figs. 3, 4 and Tables 5, 6). On the other hand, crystallization of only $K_2O{\cdot}2ZnO{\cdot}3B_2O_3$ occurred in KZB. These observations underline the differences between the two groups of glasses mentioned above.

Phase separation could be a reason for the occurrence of up to four crystalline phases in the glasses LZB and NZB during heating. Phase separation is well known for binary zinc borate glass melts with up to 50 mol% ZnO [54–56]. The partial substitution of ZnO by Na_2O in ZnO-B_2O_3 glasses reduces the tendency to phase separation [54]. In the as-received glasses under study here no indication of phase separation was observed. Even an analysis of the NZB glass with TEM [57] did not indicate phase separation. For KZB phase separation can be excluded because the formed phase is close to the glass composition.

5. Conclusion

i.) Regarding their potential application as sintering aids all glasses under study are qualified since crystallization did not hinder densification. LZB, NZB, KZB, RZB show only small differences in viscosity, thus sintering behavior, and could be fully densified below 540 °C during heating at 5 K/min. The viscosity curves are shifted to about 100 K lower temperatures for the alkali zinc borate glasses compared to CaZB due to higher "crosslinking" potential and coordination number of Ca^{2+}. However, they did not reach the low viscosity of their lead bearing isocompositional counterpart (LPbB) due to lower field strength of Pb^{2+} compared to Zn^{2+}.

ii.) Regarding the role and influence of network modifiers and intermediate oxides the number of fourfold coordinated boron atoms (N_4) is the essential structural parameter. Alkali containing glasses reveal a decrease of viscosity and sintering range with decreasing N_4 and increasing ionic radius.

iii.) The zinc borate glasses under study possess high fragilities (> 76). However, NZB, KZB, and even CaZB indicate no significant changes in fragility, since N_4 is almost similar.

iv.) All glasses undergo crystallization, in which the type of network modifier determines the occurring crystalline phases. In any case, zinc borates were detected including zinc orthoborate, zinc diborate and zinc metaborate. It is interesting to note, that zinc orthoborate is a major crystal phase in LZB, NZB, and NZCuB, although its chemical composition deviates more from the glass composition than the compositions of the other crystal phases. The unique ternary crystal phase $KZnB_3O_6$ ($K_2O{\cdot}2ZnO{\cdot}3B_2O_3$) was detected in the crystallized KZB glass. The Weinberg glass stability parameter (K_W) varies between 0.07 for LZB and 0.12 for NZCuB. The different crystal phases and varying melting points of even the same crystalline phase in different glass matrices cause the span of K_W. Substitution of Zn^{2+} by Pb^{2+} or Cu^{2+} enables an improvement of glass stability.

Data availability statement

The data that support the findings of this study are available from the corresponding author upon reasonable request.

CRediT authorship contribution statement

Lina Heuser: Conceptualization, Data curation, Formal analysis, Investigation, Methodology, Validation, Visualization, Writing – original draft, Writing – review & editing. **Marianne Nofz:** Conceptualization, Visualization, Writing – original draft, Writing – review & editing. **Ralf Müller:** Conceptualization, Supervision, Funding acquisition, Visualization, Writing – original draft.

Declaration of Competing Interest

The authors declare that they have no known competing financial interests or personal relationships that could have appeared to influence the work reported in this paper.

Acknowledgement

The financial support of the Deutsche Forschungsgemeinschaft (DFG) in the research project MU 963/17-1 is gratefully acknowledged. The authors sincerely thank S. Rüster and S. Gersdorf for sample preparation, D. Al-Sabbagh for XRD, F. Lindemann for particle size measurements, C. Meyer for viscosity measurements, and S. Reinsch for DTA and gas release measurements. Special thanks go to an unknown reviewer for the valuable comments which contributed to the improvement of the manuscript.

References

[1] N.M. Bobkova, S.A. Khot'ko, Structure of zinc-borate low-melting glasses derived from IR spectroscopy data, J. Appl. Spectrosc. 72 (6) (2005) 853–857, https://doi.org/10.1007/s10812-006-0015-2.

[2] N.H. Afrizal, N. Yahya, N.M. Yusoff, A. Kasim, A. Hashim, Physical, mechanical and structural properties of yttrium oxide doped zinc borate glasses, Solid State

Phenom. 307 (2020) 327–335, https://doi.org/10.4028/www.scientific.net/SSP.307.327.
[3] N.M. Bobkova, S.A. Khot'ko, Zinc oxide in borate glass-forming systems, Glas. Ceram. 62 (5–6) (2005) 167–170, https://doi.org/10.1007/s10717-005-0064-7.
[4] M. Eberstein, U. Schmidt, S. Körner, K. Reinhardt, R. Jurk, U. Partsch, In-situ observations of glass frit related effects during the front side paste contact formation, in: D. Abbott (Ed.), 2014 IEEE 40th Photovoltaic Specialist Conference (PVSC), IEEE, Denver, USA, 2014, pp. 3463–3469, https://doi.org/10.1109/PVSC.2014.6925678.
[5] S. Körner, M. Eberstein, WO 2016/062820 A1, Method for producing a silver-containing glass powder, and use of the glass powder. Fraunhofer-Gesellschaft zur Förderung der angewandten Forschung e.V, 2016.
[6] S. Körner, Lösungs-und Ausscheidungsprozesse in silberhaltigen Glasschmelzen bei der thermischen Kontaktierung von multikristallinem Silicium, Technische Universität Dresden, 2018.
[7] A. Sayyadi-Shahraki, E. Taheri-Nassaj, S.A. Hassanzadeh-Tabrizi, H. Barzegar-Bafrooei, Low temperature cofirable $Li_2Zn_3Ti_4O_{12}$ microwave dielectric ceramic with Li_2O-ZnO-B_2O_3 glass additive, J. Mater. Sci. Mater. Electron. 25 (1) (2014) 355–360, https://doi.org/10.1007/s10854-013-1594-3.
[8] G. Chen, M. Hou, Y. Bao, C. Yuan, C. Zhou, H. Xu, Silver co-Firable $Li_2ZnTi_3O_8$ microwave dielectric ceramics with LZB glass additive and TiO_2 dopant, Int. J. Appl. Ceram. Technol. 10 (3) (2013) 492–501, https://doi.org/10.1111/j.1744-7402.2012.02754.x.
[9] S. Danewalia, K. Singh, S. Arya, Influence of vanadium oxide on non-isothermal crystallization kinetics of zinc lithium borate glasses, J. Non-Cryst. Solids 553 (2021), 120471, https://doi.org/10.1016/j.jnoncrysol.2020.120471.
[10] A. Saidu, H. Wagiran, M.A. Saeed, Y.S.M. Alajerami, Structural properties of zinc lithium borate glass, Opt. Spectrosc. 117 (3) (2014) 396–400, https://doi.org/10.1134/S0030400x14090239.
[11] M.S. Gaafar, N.S. Abd El-Aal, O.W. Gerges, G. El-Amir, Elastic properties and structural studies on some zinc-borate glasses derived from ultrasonic, FT-IR and X-ray techniques, J. Alloys Compd. 475 (1–2) (2009) 535–542, https://doi.org/10.1016/j.jallcom.2008.07.114.
[12] L. Heuser, M. Nofz, Alkali and alkaline earth zinc and lead borate glasses: structure and properties, J. Non-Crystal. Solids: X (2022), 100109, https://doi.org/10.1016/j.nocx.2022.100109.
[13] FIZ Karlsruhe GmbH, Inorganic Crystal Structure Database (ICSD), Eggenstein-Leopoldshafen, Germany, 2019.
[14] Deutsches Institut für Normung e.V., DIN 53019-1, Viskosimetrie – Messung von Viskositäten und Fließkurven mit Rotationsviskosimetern – Teil 1, Grundlagen und Messgeometrie, Berlin, 2008.
[15] Deutsches Institut für Normung e.V., DIN ISO 7884-2, Glas – Viskosität und viskosimetrische Festpunkte – Teil 2, Bestimmung der Viskosität mit Rotationsviskosimetern, Berlin, 1998.
[16] ASTM International, ASTM C1351M − 96 (Reapproved 2017), Standard Test Method for Measurement of Viscosity of Glass Between 10^4 Pa·s and 10^8 Pa·s by Viscous Compression of a Solid Right Cylinder [Metric][1], West Conshohocken, United States, 1996, 2017.
[17] J.C. Mauro, Y. Yue, A.J. Ellison, P.K. Gupta, D.C. Allan, Viscosity of glass-forming liquids, Proc. Natl. Acad. Sci. U. S. A. 106 (47) (2009) 19780–19784, https://doi.org/10.1073/pnas.0911705106.
[18] O.V. Mazurin, Yu.V. Gankin, Glass transition temperature: problems of measurement procedures, Glass Technol.-Eur. J. Glass Sci. Technol. Part A 49 (5) (2008) 229–233.
[19] R. Müller, S. Reinsch, Viscous-phase silicate processing, in: N.P. Bansal, A. R. Boccaccini (Eds.), Ceramics and Composites Processing Methods, John Wiley & Sons Inc., Hoboken, New Jersey, 2012, pp. 75–144, https://doi.org/10.1002/9781118176665.ch3.
[20] A. Winkel, R. Meszaros, S. Reinsch, R. Müller, N. Travitzky, T. Fey, P. Greil, L. Wondraczek, Sintering of 3 D-printed glass/HAp composites, J. Am. Ceram. Soc. 95 (11) (2012) 3387–3393, https://doi.org/10.1111/j.1551-2916.2012.05368.x.
[21] X. Chen, H. Xue, X. Chang, L. Zhang, Y. Zhao, J. Zuo, H. Zang, W. Xiao, Syntheses and crystal structures of the α- and β-forms of zinc orthoborate, $Zn_3B_2O_6$, J. Alloys Compd. 425 (1–2) (2006) 96–100, https://doi.org/10.1016/j.jallcom.2006.01.068.
[22] S. Garcia-Blanco, J. Fayos, The crystal structure of zinc orthoborate, $Zn_3(BO_3)_2$, Z. Kristallogr. 127 (1–6) (1968) 145–159, https://doi.org/10.1524/zkri.1968.127.16.145.
[23] D. Smith, et al., ICDD Grant-in-Aid, Penn State University, University Park, PA, USA, 1974.
[24] M. Martinez-Ripoll, S. Martínez-Carrera, S. Garcia-Blanco, The crystal structure of zinc diborate ZnB_4O_7, Acta Cryst 27 (3) (1971) 672–677, https://doi.org/10.1107/S0567740871002759.
[25] D. Smith, D. Pfoertsch, L. Zellmer, B. Scheetz, ICDD Grant-in-Aid, Penn State University, University Park, PA, USA, 1987.
[26] N. Sennova, R.S. Bubnova, G. Cordier, B. Albert, S.K. Filatov, L. Isaenko, Temperature-dependent changes of the crystal structure of $Li_2B_4O_7$, Z. Anorg. Allg. Chem. 634 (14) (2008) 2601–2607, https://doi.org/10.1002/zaac.200800295.
[27] Y. Xu, S. Jin, W. Wang, X. Chen, ICDD Grant-in-Aid, Inst. of Physics, Chinese Academy of Sciences, Beijing, P.R. China, 2009.
[28] S. Jin, G. Cai, W. Wang, M. He, S. Wang, X. Chen, Stable oxoborate with edge-sharing BO_4 tetrahedra synthesized under ambient pressure, Angew. Chem. 122 (29) (2010) 5087–5090, https://doi.org/10.1002/ange.200907075.
[29] B. Agea-Blanco, S. Reinsch, R. Müller, Sintering and foaming of barium silicate glass powder compacts, Front. Mater. 3 (45) (2016), https://doi.org/10.3389/fmats.2016.00045.
[30] R. Müller, H. Behrens, B. Agea-Blanco, S. Reinsch, T. Wirth, Foaming species and trapping mechanisms in barium silicate glass sealants, Adv. Eng. Mater. 24 (2022) 2100445, https://doi.org/10.1002/adem.202100445.
[31] C. Blaeß, R. Müller, Sintering and foaming of bioactive glasses, J. Am. Ceram. Soc. n/a (2022) 1–11, https://doi.org/10.1111/jace.18626.
[32] H. Scholze, Glass - Nature, Structure and Properties, Springer-Verlag, New York, Berlin, Heidelberg, 1991, p. 168.
[33] G.D. Chryssikos, E.I. Kamitsos, Y.D. Yiannopoulos, Towards a structural interpretation of fragility and decoupling trends in borate systems, J. Non-Cryst. Solids 196 (1996) 244–248, https://doi.org/10.1016/0022-3093(95)00594-3.
[34] Y.D. Yiannopoulos, G.D. Chryssikos, E.I. Kamitsos, Structure and properties of alkaline earth borate glasses, Phys. Chem. Glasses 42 (3) (2001) 164–172.
[35] G.D. Chryssikos, E.I. Kamitsos, M.A. Karakassides, Structure of borate glasses. Part 2. Alkali induced network modifications in terms of structure and properties, Phys. Chem. Glasses 31 (3) (1990) 109–116.
[36] E.I. Kamitsos, G.D. Chryssikos, Borate glass structure by Raman and infrared spectroscopies, J. Mol. Struct. 247 (1991) 1–16, https://doi.org/10.1016/0022-2860(91)87058-P.
[37] E.I. Kamitsos, Modifying role of alkali-metal cations in borate glass networks, J. Phys. Chem. 93 (4) (1989) 1604–1611, https://doi.org/10.1021/j100341a083.
[38] N. Uchida, T. Maekawa, T. Yokokawa, Hard basicity of borate anion clusters, J. Non-Cryst. Solids 88 (1) (1986) 1–10, https://doi.org/10.1016/S0022-3093(86)80083-7.
[39] Z.Y. Yao, D. Möncke, E.I. Kamitsos, P. Houizot, F. Célarié, T. Rouxel, L. Wondraczek, Structure and mechanical properties of copper-lead and copper-zinc borate glasses, J. Non-Cryst. Solids 435 (2016) 55–68, https://doi.org/10.1016/j.jnoncrysol.2015.12.005.
[40] A. Napolitano, P.B. Macedo, E.G. Hawkins, Viscosity and density of boron trioxide, J. Am. Ceram. Soc. 48 (12) (1965) 613–616, https://doi.org/10.1111/j.1151-2916.1965.tb14690.x.
[41] P.B. Macedo, A. Napolitano, Inadequacies of viscosity theories for B_2O_3, J. Chem. Phys. 49 (4) (1968) 1887–1895, https://doi.org/10.1063/1.1670321.
[42] C.A. Angell, Spectroscopy simulation and scattering, and the medium range order problem in glass, J. Non-Cryst. Solids 73 (1–3) (1985) 1–17, https://doi.org/10.1016/0022-3093(85)90334-5.
[43] C.A. Angell, Formation of glasses from liquids and biopolymers, Science 267 (5206) (1995) 1924–1935, https://doi.org/10.1126/science.267.5206.1924.
[44] D.L. Sidebottom, Connecting glass-forming fragility to network topology, Front. Mater. 6 (144) (2019), https://doi.org/10.3389/fmats.2019.00144.
[45] Y. Matsuda, Y. Fukawa, M. Kawashima, S. Mamiya, S. Kojima, Dynamic glass transition and fragility of lithium borate binary glass, Solid State Ionics 179 (40) (2008) 2424–2427, https://doi.org/10.1016/j.ssi.2008.09.011.
[46] J.C. Mauro, P.K. Gupta, R.J. Loucks, Composition dependence of glass transition temperature and fragility. II. A topological model of alkali borate liquids, J. Chem. Phys. 130 (2009), 234503, https://doi.org/10.1063/1.3152432.
[47] L. Shartsis, W. Capps, Surface tension of molten alkali borates, J. Am. Ceram. Soc. 35 (7) (1952) 169–172, https://doi.org/10.1111/j.1151-2916.1952.tb13094.x.
[48] H. Scholze, Der Einfluss von Viskosität und Oberflächenspannung auf erhitzungsmikroskopische Messungen an Gläsern, Ber. Dtsch. Keram. Ges 39 (1) (1962) 63–68.
[49] M.C. Weinberg, An assessment of glass stability criteria, Phys. Chem. Glasses 35 (3) (1994) 119–123.
[50] M.L.F. Nascimento, L.A. Souza, E.B. Ferreira, E.D. Zanotto, Can glass stability parameters infer glass forming ability? J. Non-Cryst. Solids 351 (40–42) (2005) 3296–3308, https://doi.org/10.1016/j.jnoncrysol.2005.08.013.
[51] E.B. Ferreira, E.D. Zanotto, S. Feller, G. Lodden, J. Banerjee, T. Edwards, M. Affatigato, Critical analysis of glass stability parameters and application to lithium borate glasses, J. Am. Ceram. Soc. 94 (11) (2011) 3833–3841, https://doi.org/10.1111/j.1551-2916.2011.04767.x.
[52] A. Whitaker, Temperature dependence of the stability of zinc borates, J. Mater. Sci. 7 (2) (1972) 189–193.
[53] L. Yang, W. Fan, Y. Li, H. Sun, L. Wei, X. Cheng, X. Zhao, Theoretical insight into the structural stability of $KZnB_3O_6$ polymorphs with different BO_x polyhedral networks, Inorg. Chem. 51 (12) (2012) 6762–6770, https://doi.org/10.1021/ic300469s.
[54] D. Ehrt, Zinc and manganese borate glasses–phase separation, crystallisation, photoluminescence and structure, Phys. Chem. Glasses Eur. J. Glass Sci. Technol. B 54 (2) (2013) 65–75.
[55] E.M. Levin, S. Block, Structural interpretation of immiscibility in oxide systems: I, analysis and calculation of immiscibility, J. Am. Ceram. Soc. 40 (3) (1957) 95–106, https://doi.org/10.1111/j.1151-2916.1957.tb12583.x.
[56] M. Bengisu, Borate glasses for scientific and industrial applications: a review, J. Mater. Sci. Mater. Electron. 51 (5) (2016) 2199–2242, https://doi.org/10.1007/s10853-015-9537-4.
[57] L. Heuser, A. Guilherme Buzanich, M. Radtke, L. Agudo Jácome, I. Feldmann, J. Deubener, Silver diffusion in low-melting alkali zinc borate model glasses studied by means of SNMS, TEM and XAS - conference talk, 94. Glastechnische Tagung, Online, 2021.